Inorganic Chemistry
Article

Inorg. Chem. **2010**, *49*, 997–1007 **997**
DOI: 10.1021/ic9019684

Octahedral Copper(II) and Tetrahedral Copper(I) Double-Strand Helicates: Chiral Self-Recognition and Redox Behavior

Valeria Amendola,[†] Massimo Boiocchi,[‡] Valentina Brega,[†] Luigi Fabbrizzi,*[,†] and Lorenzo Mosca[†]

[†]*Dipartimento di Chimica Generale and* [‡]*Centro Grandi Strumenti, Università di Pavia, 27100 Pavia, Italy*

Received October 5, 2009

The racemic form of **5** (^{RR}**5** + ^{SS}**5**) gives dinuclear complexes of 2:2 stoichiometry both with Cu^{II}, acting as a bis-terdentate ligand, and with Cu^{I}, acting as a bis-bidentate ligand. Single crystal X-ray diffraction studies have shown that the Cu^{II} complex exists as double-strand homochiral helicate molecules: *P*,*P*-$[Cu_2^{II}(^{RR}\mathbf{5})_2]^{4+}$ and *M*,*M*-$[Cu_2^{II}(^{SS}\mathbf{5})_2]^{4+}$; in which the two *trans*-1,2-cyclohexanediamine subunits have the same chirality for of the two strands. Each Cu^{II} metal center is six-coordinated according to a *cis*-octahedral geometry and interacts with a NNO donor subunit of each strand. The Cu^{I} complex, when crystallized from THF in the presence of ^{rac}**5**, gives a double-strand homochiral helicate complex and in the solid state forms a racemic mixture of the homochiral metal complexes *M*,*M*-$[Cu_2^{I}(^{RR}\mathbf{5})_2]^{2+}$ and *P*,*P*-$[Cu_2^{I}(^{SS}\mathbf{5})_2]^{2+}$. When crystallizing from a MeCN solution, Cu^{I} and ^{rac}**5** give rise to the heterochiral nonhelicate dimeric complex $[Cu_2^{I}(^{RR}\mathbf{5})(^{SS}\mathbf{5})]^{2+}$, in which the two strands of the dimer have inverse configuration of the *trans*-1,2-cyclohexanediamine subunits and are assembled side-by-side. In both structural architectures, the Cu^{I} centers are four-coordinated by two nitrogen atoms from each strand, according to a distorted tetrahedral geometry. In MeCN solution, the dinuclear Cu^{II} complex disassembles to give the mononuclear species, which, on reduction at a platinum electrode in a cyclic voltammetry experiment, gives two Cu^{I} mononuclear complexes that quickly assemble to give the dinuclear Cu^{I} complex. This complex undergoes two consecutive one-electron oxidation processes, but the dinuclear Cu^{II} species that forms decomposes in less than 1 s. On the contrary, the $[Cu_2^{I}(^{rac}\mathbf{5})_2]^{2+}$ complex is stable in MeCN solution and undergoes two one-electron oxidation processes to give a form of dinuclear Cu^{II} complex that lasts in solution for more than 20 s.

Introduction

Objects arranged in a double-strand helical shape have attracted and intrigued human beings for a long time. One of the first examples refers to the *caduceus*, "the staff of the herald", belonging to the Greek god Hermes (Mercury for Latins), a winged rod with two snakes wrapped around in a double helical mode, which is present in any painting or sculpture featuring Hermes/Mercury from Hellenic art to the Renaissance (Figure 1a).[1] The double helix has also represented an ambitious task in architecture: a spectacular example is provided by Saint Patrick's well in Orvieto, Italy, constructed by the architect/engineer Antonio da Sangallo the Younger during the period 1527−1537. The well is 53 m deep and 14 m wide and is equipped with a pair of wide spiral staircases, lit by 72 internal windows, which form a double helix, so that mules laden with water-jars could descend on one ramp and come back up the other, without colliding.

After Crick and Watson's disclosure of the structure of DNA,[2] the double helix has become a recurring and captivating motif of the molecular world and chemical design. In 1987, Lehn reported the first example of "inorganic double helices", i.e. a series of Cu^{I} polynuclear metal complexes (helicates), in which two linear multidentate ligands are wrapped around two or more metals, forming a double helix.[3] Both DNA and helicates are held together by noncovalent interactions (hydrogen bonding and metal−ligand interactions, respectively), a feature that allows the reversible assembling to give an elaborate structure, through a repetitive trial-and-error mechanism. The formation of dinuclear to tetranuclear double helicates is usually a fast process, in which the thermodynamic equilibrium is reached over a period ranging from seconds to minutes. However, double helicates of higher nuclearity, especially in the presence of bulky substituents on the ligand backbone, may reach the termodynamic equilibrium over a period of hours and days.[4]

The double helical structure of helicate complexes results from the fine balance between (i) the coordinative geometrical

*To whom correspondence should be addressed. E-mail: luigi.fabbrizzi@unipv.it.

(1) Fabbrizzi, L. *J. Chem. Educ.* **2008**, *85*, 1501–1511.
(2) Watson, J. D.; Crick, F. H. C. *Nature* **1953**, *171*, 737–738.
(3) Lehn, J.-M.; Rigault, A.; Siegel, J.; Harrowfield, J.; Chevrier, B.; Moras, D. *Proc. Natl. Acad. Sci. U.S.A.* **1987**, *84*, 2565–2569.
(4) Marquis-Rigault, A.; Dupont-Gervais, A.; Van Dorsselaer, A.; J.-M. Lehn, J.-M. *Chem.—Eur. J.* **1996**, *2*, 1395–1398.

Published on Web 12/23/2009

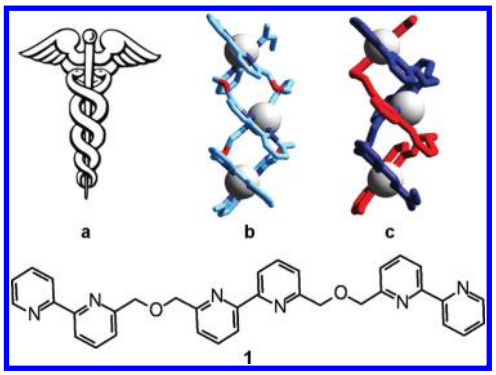

Figure 1. (a) Caduceus, the staff of the god Hermes/Mercury, featuring two snakes intertwined in a double-helical arrangement. (b) Molecular structure of the trimetallic double-strand helicate complex $[Ag_3^I(\mathbf{1})_2]^{3+}$.[5] (c) Same structure as in part b, but with the two strands represented in different colors, blue and red. Ag^I metal centers are represented as spheres. The hydrogen atoms of the two strands have been omitted for clarity. Structures are redrawn from data deposited at the Cambridge Crystallographic Data Center: CCDC 1628.

preferences of the metal center and (ii) the steric constraints present in the linear ligand, which may contrast the formation of a mononuclear complex. Mononuclear tetrahedral and octahedral complexes already possess a *helical twist* and are good candidates for the formation of helicates.[5] In fact, first double-stranded helicates were obtained with d^{10} metal ions (Cu^I, Ag^I), which have a strong preference for tetrahedral coordination geometry.[6] Metals prone to octahedral coordination, e.g. Ni^{II}, Co^{II}, will form double-strand helicates with ligand bearing terdentate subunits (or triple stranded helicates, if the ligand possesses bidentate coordinating subunits).[7]

Copper is a special case, when in the presence of a tetradentate ligand **L**. In fact, the Cu^I state will form the stable dinuclear double-strand helicate $[Cu_2^I(\mathbf{L})_2]^{2+}$. On the other hand, the Cu^{II} state likes square coordination, a geometrical arrangement which does not possess the helical twist and, in the absence of particular sterical constraints, will tend to form a mononuclear complex, $[Cu^{II}(\mathbf{L})]^{2+}$, of square geometry (or a geometry related to the square: square pyramid, elongated octahedron). These contrasting features may give rise to an interesting behavior associated to the Cu^{II}/Cu^I redox change, which is pictorially illustrated in Figure 2.

In fact, on Cu^{II}-to-Cu^I reduction, the two mononuclear complexes will assemble to form the dinuclear helicate complex, whereas, on Cu^I-to-Cu^{II} oxidation, the helicate will disassemble to regenerate the two mononuclear complexes. The first example of this unique redox driven

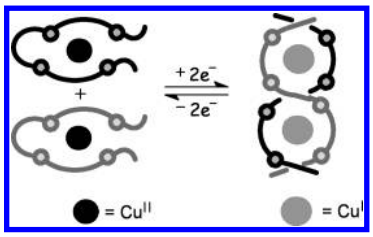

Figure 2. Redox driven assembling−disassembling of a dicopper(I) double-strand helicate complex.

assembling−disassembling process was observed with the quadridentate ligand **2**.[8]

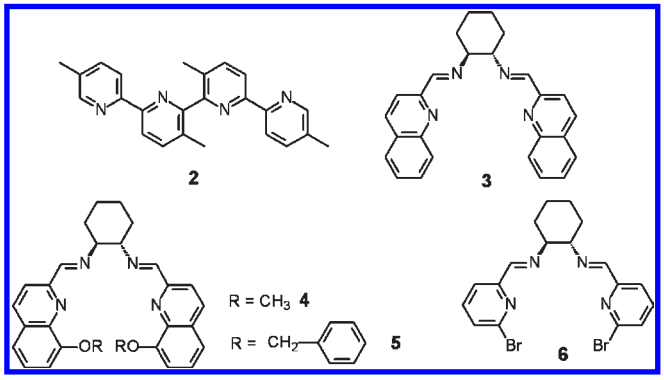

X-ray diffraction studies showed that, in the solid state, Cu^I gives the dimeric complex $[Cu_2^I(\mathbf{2})_2]^{2+}$, in which two quaterpyridine ligands are arranged in a double helical mode,[9] whereas Cu^{II} forms a monomeric complex of formula $[Cu^{II}(\mathbf{2})(H_2O)]^{2+}$, exhibiting a square pyramidal geometry, with the water molecule occupying the apical position.[8] The redox driven assembling−disassembling process was investigated through cyclic voltammetry (CV) studies in an MeCN solution.[8] On reduction of the $[Cu^{II}(\mathbf{2})]^{2+}$ complex, a single wave developed; on the reverse oxidation scan, two one-electron waves, separated by 400 mV, were observed. This indicates that, following Cu^{II}-to-Cu^I reduction, two monomeric complexes assemble to give the dimeric helicate species, $[Cu_2^I(\mathbf{2})_2]^{2+}$. This species undergoes stepwise one-electron oxidation to $[Cu^I, Cu^{II}(\mathbf{2})_2]^{3+}$ and $[Cu_2^{II}(\mathbf{2})_2]^{4+}$. The latter dimeric dicopper(II) species is stable over the time scale of the CV experiment. In fact, in the following reduction scan, two consecutive waves, separated by 400 mV, developed. This study prompted several researchers to investigate the Cu^{II}/Cu^I redox change in helicate complexes with a variety of multidentate ligands.[10] Different CV patterns were observed, depending upon the structural features of the helicand (denticity, rigidity, steric hindrance). In some cases, the mixed valence Cu^I/Cu^{II} helicate complex was stabilized by a definite metal−metal interaction and could be isolated in the solid state and structurally characterized through X-ray diffraction studies.[11] Structural aspects of helicate metal

(5) Albrecht, M. *Chem. Rev.* **2001**, *101*, 3457–3497.
(6) (a) Garrett, T. M.; Koert, U.; Lehn, J.-M.; Rigault, A.; Meyer, D.; Fischer, J. *Chem. Commun.* **1990**, 557–558. (b) Barley, M.; Constable, E. C.; Corr, S. A.; McQueen, R. C. S.; Nutkins, J. C.; Ward, M. D.; Drew, M. G. B. *J. Chem. Soc., Dalton Trans.* **1988**, 2655–2662. (c) Piguet, C.; Bernardinelli, G.; Williams, A. F. *Inorg. Chem.* **1989**, *28*, 2920–2925.
(7) (a) Piguet, C.; Bernardinelli, G.; Bocquet, B.; Quattropani, A.; Williams, A. F. *J. Am. Chem. Soc.* **1992**, *114*, 7440–7451. (b) Krämer, R.; Lehn, J.-M.; DeCian, A.; Fischer, J. *Angew. Chem., Int. Ed. Engl.* **1993**, *32*, 703–706.
(8) Gisselbrecht, J.-P.; Gross, M.; Lehn, J.-M.; Sauvage, J.-P.; Ziessel, R.; Piccinni-Leopardi, C.; Arrieta, J. M.; Germain, G.; Van Meerssche, M. *Nouv. J. Chim.* **1984**, *8*, 661–667.
(9) Lehn, J.-M.; Sauvage, J.-P.; Simon, J.; Ziessel, R.; Piccini-Leopardi, C.; Germain, G.; G., Declercq, J.-P.; Van Meersche, M. *Nouv. J. Chim.* **1983**, *7*, 413–420.
(10) (a) Yao, Y.; Perkovic, M. W.; Rillema, D. P.; Woods, C. *Inorg. Chem.* **1992**, *31*, 3956–3962. (b) Potts, K. T.; Keshavarz-K, M.; Tham, F. S.; Abruña, H. D.; Arana, C. R. *Inorg. Chem.* **1993**, *32*, 4422–4435. (c) Potts, K. T.; Keshavarz-K, M.; Tham, F. S.; Abruña, H. D.; Arana, C. R. *Inorg. Chem.* **1993**, *32*, 4450–4456. (d) Ziessel, R.; Harriman, A.; Suffert, J.; Youinou, M. T.; De Cian, A.; Fischer, J. *Angew. Chem., Int. Ed. Engl.* **1997**, *36*, 2509–2511.
(11) Jeffery, J. C.; Riis-Johannessen, T.; Anderson, C. J.; Adams, C. J.; Robinson, A.; Argent, S. P.; Ward, M. D.; Rice, C. R. *Inorg. Chem.* **2007**, *46*, 2417–2426.

complexes have been discussed in comprehensive reviews and highlights.[5,12]

We entered the intriguing world of copper helicates with the bis-bidentate ligand **3**, which could be easily obtained through Schiff base condensation of *trans*-1,2-cyclohexanediamine (racemic form) with 2-quinoline-carbaldehyde.[13,14] X-ray diffraction studies indicated that the Cu^{II} ion forms a monomeric complex of slightly distorted square geometry.[13] On the other hand, in the $[Cu_2^{I}(^{rac}\mathbf{3})_2](CF_3SO_3)_2$ complex salt, the two metal centers are tetrahedrally coordinated by the two ligands intertwined in a double helical arrangement, to form the racemic mixture of homochiral complexes *M*,*M*-$[Cu_2^{I}(^{RR}\mathbf{3})_2]^{2+}$ (i.e., a double helix with *M* handedness) and *P*,*P*-$[Cu_2^{I}(^{SS}\mathbf{3})_2]^{2+}$ (i.e., a double helix with *P* handedness).[13] Quite interestingly, in the crystal of the perchlorate salt $[Cu_2^{I}(^{rac}\mathbf{3})_2](ClO_4)_2$, both the enantiomeric forms of the dimeric homochiral helical species *M*,*M*-$[Cu_2^{I}(^{RR}\mathbf{3})_2]^{2+}$ and *P*,*P*-$[Cu_2^{I}(^{SS}\mathbf{3})_2]^{2+}$ coexist with the dimeric heterochiral non-helical (side-by-side) form $[Cu_2^{I}(^{SS}\mathbf{3})(^{RR}\mathbf{3})]^{2+}$ in a 2:1 ratio, indicating a close stability of the two arrangements in the $[Cu_2^{I}(^{rac}\mathbf{3})_2]^{2+}$ dinuclear complex.[13]

CV studies on a MeCN solution of the $[Cu_2^{I}(^{rac}\mathbf{3})_2]^{2+}$ complex showed a single irreversible wave, both in the oxidation and in the reduction scan. Such a response indicated the occurrence of a fast disassembling-assembling equilibrium even in the time scale of the CV experiments.[13] More recently, Pallavicini et al. investigated the redox behavior of the copper complexes of **4** (*R* form) in which a methoxy group had been appended in position 8 of the quinoline moiety of **3**.[15] The $[Cu^{II}(\mathbf{4})]^{2+}$ complex showed in MeCN the same CV behavior of $[Cu^{II}(\mathbf{2})]^{2+}$: one single peak in the reduction scan, and two peaks separated by 250 mV in the following oxidation scan. The tendency to form the double-strand helicate complex was confirmed by the crystal structure determination of the homochiral *M*,*M*-$[Cu_2^{I}(^{RR}\mathbf{3})_2]^{2+}$ double helicate complex.[15]

We are now considering the Schiff base derivative **5**, in which a benzyloxy group has been appended in 8 at the quinoline moiety. The aims of the present work are (i) to verify whether the oxygen atom on each benzyloxy group can act as a donor atom; if yes, each strand would contain two terdendate subunits and should be available to form helicate complexes with metals liking octahedral, even if distorded geometry (including Cu^{II}); (ii) to ascertain whether the benzyl pendant can be involved in a $\pi-\pi$ interaction with an aromatic ring of the other strand, thus providing an additional contribution to the formation of the double helix; and (iii) to evaluate the effects of i and ii, if any, on the electrochemical behavior of Cu^{II} and Cu^{I} complexes with **5**.

A further element of interest is related to the chiral properties of the investigated double-strand helicate complexes. In fact, **5** was obtained from Schiff base condensation of the racemic *trans*-1,2-cyclohexanediamine with the pertinent aldehyde and was therefore a mixture of the two enantiomeric *R*,*R* and *S*,*S* forms. Stack et al. have reported that the racemic mixture of the analogous ligand **6**, obtained from Schiff base condensation of *trans*-1,2-cyclohexanediamine with the pertinent 2-pyridine-aldehyde, reacts with copper(I) ions to give only a racemic mixture of the homochiral double helicate species: *M*,*M*-$[Cu_2^{I}(^{RR}\mathbf{6})_2]^{2+}$ and *P*,*P*-$[Cu_2^{I}(^{SS}\mathbf{6})_2]^{2+}$ through "chiral-directed self-assembling".[16] In the present work, a double-strand helicate complex was obtained also with the Cu^{II} cation, showing a local octahedral coordination geometry. This allowed us to extend the principle of homochiral recognition to helicates exhibiting octahedral coordination geometry. Moreover, dicopper(I) complexes of **5** were obtained both in the helicate and in the side-by-side forms, depending upon crystallization conditions. This provided the opportunity to verify if and how chirality controls the geometrical arrangement of dicopper(I) complexes with bis-bidendate ligands derived from *trans*-1,2-cyclohexanediamine. Diastereoselective self-assembling of dinuclear copper helicates with chiral bis-bidentate ligands of varying nature (based in particular on 2,2′-bipyridines[17] and on ter- and quaterpyridines)[18] represents a classical topic of supramolecular chemistry and has been extensively investigated over the last two decades.

Experimental Section

General Procedures and Materials. All reagents for syntheses were purchased form Aldrich/Fluka and used without further purification. $[Cu^{I}(CH_3CN)_4]ClO_4$ was prepared by a literature method[19] and recrystallized from MeCN prior to use. All reactions were performed under N_2.

UV/vis spectra were recorded on a Varian CARY 100 spectrophotometer with quartz cuvettes of the appropriate path length (0.1 or 1 cm). In any case, the concentration of the chromophore and the optical path were adjusted in order to obtain spectra with AU $\leq$ 1.

^{1}H NMR were obtained, at 298 K, on a Bruker Avance 400 spectrometer (400 MHz) operating at 9.37 T. Mass spectra were acquired on a Thermo-Finnigan ion trap LCQ Advantage Max

(12) (a) Piguet, C.; Bernardinelli, G.; Hopfgartner, G. *Chem. Rev.* **1997**, *97*, 2005–2062. (b) Piguet, C.; Borkovec, M.; Hamacek, J.; Zeckert, K. *Coord. Chem. Rev.* **2005**, *249*, 705–726. (c) Albrecht, M. *Angew. Chem., Int. Ed.* **2005**, *44*, 6448–6451.

(13) Amendola, V.; Fabbrizzi, L.; Linati, L.; Mangano, C.; Pallavicini, P.; Pedrazzini, V.; Zema, M. *Chem.—Eur. J.* **1999**, *5*, 3679–3688.

(14) (a) Amendola, V.; Fabbrizzi, L.; Mangano, C.; Pallavicini, P.; Roboli, E.; Zema, M. *Inorg. Chem.* **2000**, *39*, 5803–5806. (b) Amendola, V.; Fabbrizzi, L.; Pallavicini, P. *Coord. Chem. Rev.* **2001**, *216−217*, 435–448. (c) Amendola, V.; Fabbrizzi, L.; Gianelli, L.; Maggi, C.; Mangano, C.; Pallavicini, P.; Zema, M. *Inorg. Chem.* **2001**, *40*, 3579–3587. (d) Amendola, V.; Fabbrizzi, L.; Pallavicini, P.; Sartirana, E.; Taglietti, A. *Inorg. Chem.* **2003**, *42*, 1632–1636. (e) Amendola, V.; Fabbrizzi, L.; Mundum, E.; Pallavicini, P. *Dalton Trans.* **2003**, 773–774.

(15) Pallavicini, P.; Boiocchi, M.; Dacarro, G.; Mangano, C. *New J. Chem.* **2007**, *31*, 927–935.

(16) Masood, M. A.; Enemark, E. J.; Stack, T. D. P. *Angew. Chem., Int. Ed.* **1998**, *37*, 928–932.

(17) (a) Zarges, W.; Hall, J.; Lehn, J.-M.; Bolm, C. *Helv. Chim. Acta* **1991**, *74*, 1843–1852. (b) Woods, C. R.; Benaglia, M.; Cozzi, F.; Siegel, J. S. *Angew. Chem., Int. Ed.* **1996**, *35*, 1830–1833. (c) Baum, G.; Constable, E. C.; Fenske, D.; Housecroft, C. E.; Kulke, T. *Chem. Commun.* **1999**, 195–196. (d) Mamula, O.; von Zelewsky, A.; Bark, T.; Bernardinelli, G. *Angew. Chem., Int. Ed.* **1999**, *38*, 2945–2948. (e) Mamula, O.; Monlien, F. J.; Porquet, A.; Hopfgartner, G.; Merbach, A. E.; von Zelewsky, A. *Chem.—Eur. J.* **2001**, *7*, 533–539. (f) Annunziata, R.; Benaglia, M.; Cinquini, M.; Cozzi, F.; Woods, C. R.; Siegel, J. S. *Eur. J. Org. Chem.* **2001**, 173–180. (g) Prabaharan, R.; Fletcher, N. C.; Nieuwenhuyzen, M. *J. Chem. Soc., Dalton Trans.* **2002**, 602–608. (h) Prabaharan, R.; Fletcher, N. C. *Inorg. Chim. Acta* **2003**, *355*, 449–453. (i) Telfer, S. G.; Tajima, N.; Kuroda, R. *J. Am. Chem. Soc.* **2004**, *126*, 1408–1418. (j) Mamula, O.; von Zelewsky, A.; Brodard, P.; Schläpfer, C.-W.; Bernardinelli, G.; Stoeckli-Evans, H. *Chem.—Eur. J.* **2005**, *11*, 3049–3057.

(18) (a) Baum, G.; Constable, E. C.; Fenske, D.; Kulke, T. *Chem. Commun.* **1997**, 2043–2044. (b) Baum, G.; Constable, E. C.; Fenske, D.; Housecroft, C. E.; Kulke, T. *Chem.—Eur. J.* **1999**, *5*, 1862–1873. (c) Baum, G.; Constable, E. C.; Fenske, D.; Housecroft, E.; Kulke, T.; Neuburger, M.; Zehnder, M. *J. Chem. Soc., Dalton Trans.* **2000**, 945–959.

(19) Hathaway, J.; Holah, D. G.; Postlethwaite, J. D. *J. Chem. Soc.* **1961**, 3215–3218.

Table 1. Crystal Data for Investigated Compounds

	$[Cu_2^{II}(^{RR}\mathbf{5})_2]\,(CF_3SO_3)_4$	$[Cu_2^{II}(^{rac}\mathbf{5})_2]\,(CF_3SO_3)_4$	$[Cu_2^{I}(^{rac}\mathbf{5})_2]\,(ClO_4)_2 \cdot 2Et_2O$	$[Cu_2^{I}(^{rac}\mathbf{5})_2]\,(ClO_4)_2 \cdot H_2O$
formula	$C_{84}H_{72}Cu_2F_{12}N_8O_{16}S_4$	$C_{168}H_{144}Cu_4F_{24}N_{16}O_{32}S_8$	$C_{88}H_{92}Cl_2Cu_2N_8O_{14}$	$C_{80}H_{74}Cl_2Cu_2N_8O_{13}$
M	1932.88	3865.76	1683.70	1553.46
crystal color	brown	red	brownish blue	brown
dimension [mm]	$0.55 \times 0.43 \times 0.30$	$0.10 \times 0.05 \times 0.04$	$0.60 \times 0.50 \times 0.50$	$0.58 \times 0.25 \times 0.03$
crystal system	orthorhombic	orthorhombic	triclinic	monoclinic
space group	$P2_12_12_1$ (no. 19)	$Fddd$ (no. 70)	$P1$ (no. 2)	$P2/n$ (no. 13)
a [Å]	13.355(2)	25.986 (1)	10.568(6)	14.020(5)
b [Å]	24.720(4)	34.018(2)	13.530(6)	12.510(5)
c [Å]	25.529(3)	38.210(3)	15.543(6)	22.794(5)
α [deg]	90	90	93.88(4)	90
β [deg]	90	90	100.55(5)	103.53(1)
γ [deg]	90	90	108.20(5)	90
V [Å^3]	8428(2)	33777(4)	2057(2)	3887(2)
Z	4	8	1	2
ρ_{calcd} [g cm^{-3}]	1.523	1.520	1.359	1.327
μ $Mo_{K\alpha}$ [mm^{-1}]	0.702	0.701	0.651	0.682
scan type	ω scans	ω scans	ω scans	ω scans
θ range [deg]	2−25	2−20	2−20	2−23
measured reflections	10407	40023	4274	5667
unique reflections	9683	4118	3854	5411
R_{int}	0.017	0.092	0.108	0.046
strong data [$I_O > 2\sigma(I_O)$]	6037	2606	2045	2057
refined parameters	1135	569	514	485
$R1$, $wR2$ (strong data)	0.0593, 0.1196	0.0643, 0.1576	0.0705, 0.1585	0.1064, 0.2667
$R1$, $wR2$ (all data)	0.1127, 0.1434	0.1117, 0.1953	0.1504, 0.1927	0.2558, 0.3553
GOF	1.015	1.051	0.987	1.004
max/min residuals [e Å^{-3}]	0.38/−0.47	0.42/−0.31	0.50/−0.56	0.81/−0.37

instrument, equipped with an electrospray ionization (ESI) source.

Electrochemical measurements were performed on a BAS 100B/W instrument. MeCN was freshly distilled from CaH_2 under a N_2 atmosphere and made 0.1 M in $[Bu_4N]ClO_4$. In the CV experiments, a three-electrode cell was used with a platinum electrode as the working electrode, silver/silver ion as a reference (clean silver wire into an electrode filling solution of MeCN, made 1×10^{-2} M in $AgNO_3$ and 0.1 M in $[Bu_4N]ClO_4$) and a platinum coil as the auxiliary electrode.

Syntheses. 1,2-Cyclohexanediamine was first used in the synthesis of a helicand through Schiff base condensation with 2-pyridinecarbaldehyde.[20] Syntheses of 2-methyl-8-benzyloxyquinoline, of 8-benzyloxyquinoline-2-carbaldehyde and $^{RR}\mathbf{5}$, (1*R*,2*R*)-*N*,*N*′-bis-[1-(8-benzyloxyquinolin-2-yl)methylidene]cycloexane-1,2-diamine and $^{rac}\mathbf{5}$, (*trans*-*N*,*N*′-bis[1-(8-benzyloxyquinolin-2-yl)methylidene]-cycloexane-1,2-diamine are described in detail in the Supporting Information.

X-ray Crystallographic Studies. Diffraction data have been collected at room temperature by means of an Enraf-Nonius CAD4 four circle diffractometer equipped with a punctual detector (scintillation counter) for the $[Cu_2^{II}(^{RR}\mathbf{5})_2](CF_3SO_3)_4$, $[Cu_2^{I}(^{rac}\mathbf{5})_2](ClO_4)_2 \cdot 2Et_2O$, and $[Cu_2^{I}(^{rac}\mathbf{5})_2](ClO_4)_2 \cdot H_2O$ crystals. Only small crystals of the $[Cu_2^{II}(^{rac}\mathbf{5})_2](CF_3SO_3)_4$ molecular complex formed, and diffraction data were collected by means of a Bruker-Axs CCD-based diffractometer. All diffractometers worked with graphite-monochromatized Mo Kα X-radiation (λ = 0.71073 Å). The θ_{max} limit chosen for data collections corresponds to the value above which intensities cannot be observed with the available instrumentation. Crystal data for the molecular complexes are shown in Table 1.

Data reductions (including intensity integration, background, Lorentz, and polarization corrections) for intensities collected with the conventional diffractometer were performed with the WinGX package.[21] Absorption effects were evaluated with the psi-scan method,[22] and absorption corrections were applied to the data of $[Cu_2^{II}(^{RR}\mathbf{5})_2](CF_3SO_3)_4$ and $[Cu_2^{I}(^{rac}\mathbf{5})_2](ClO_4)_2 \cdot H_2O$ crystals: min/max transmission factors were 0.733/0.803 and 0.910/0.981, respectively. The $[Cu_2^{I}(^{rac}\mathbf{5})_2](ClO_4)_2 \cdot 2(Et_2O)$ crystal decays when placed under the X-ray beam in about 30 h. During this time, X-ray diffraction intensities were collected and the F^2 data (corrected by the effects of crystal decay) were of quality suitable for the crystallographic study. However, at the end of data collection, the psi-scan data could not be measured and absorption corrections were not applied to the diffraction data.

CCD frames collected for the $[Cu^{II}(^{rac}\mathbf{5})_2](CF_3SO_3)_4$ crystal were processed with the SAINT software[23] and intensities were corrected for Lorentz and polarization effects; absorption effects were empirically evaluated by the SADABS software,[24] and absorption correction was applied to the data (min/max transmission factors were 0.891/0.992).

All crystal structures were solved by direct methods (SIR 97),[25] and refined by full-matrix least-squares procedures on F^2 using all reflections (SHELXL 97).[26] Anisotropic displacement parameters were refined for all non-hydrogen atoms. Hydrogens were placed at calculated positions with the appropriate AFIX instructions and refined using a riding model. CCDC 740587, 740588, 740589, and 740590 contain the supplementary crystallographic data for this paper. These data can be obtained free of charge from The Cambridge Crystallographic Data Centre via www.ccdc.cam.ac.uk/data_request/cif.

(20) Van Stein, G. C.; Van der Poel, H.; Van Koten, G.; Spek, A. L.; Duisenberg, A. J. M.; Pregosin, P. S. *J. Chem. Soc., Chem. Commun.* **1980**, 1016–1018.

(21) Farrugia, L. J. *J. Appl. Crystallogr.* **1999**, *32*, 837–838.

(22) North, A. C. T.; Phillips, D. C.; Mathews, F. S. *Acta Crystallogr.* **1968**, *A24*, 351–359.

(23) *SAINT Software Reference Manual*, version 6; Bruker AXS Inc.: Madison, WI, 2003.

(24) Sheldrick, G. M. *SADABS Siemens Area Detector Absorption Correction Program*; University of Göttingen: Göttingen, Germany, 1996.

(25) Altomare, A.; Burla, M. C.; Camalli, M.; Cascarano, G. L.; Giacovazzo, C.; Guagliardi, A.; Moliterni, A. G. G.; Polidori, G.; Spagna, R. *J. Appl. Crystallogr.* **1999**, *32*, 115–119.

(26) Sheldrick, G.M. *SHELX97 Programs for Crystal Structure Analysis*; University of Göttingen: Göttingen, Germany, 1997.

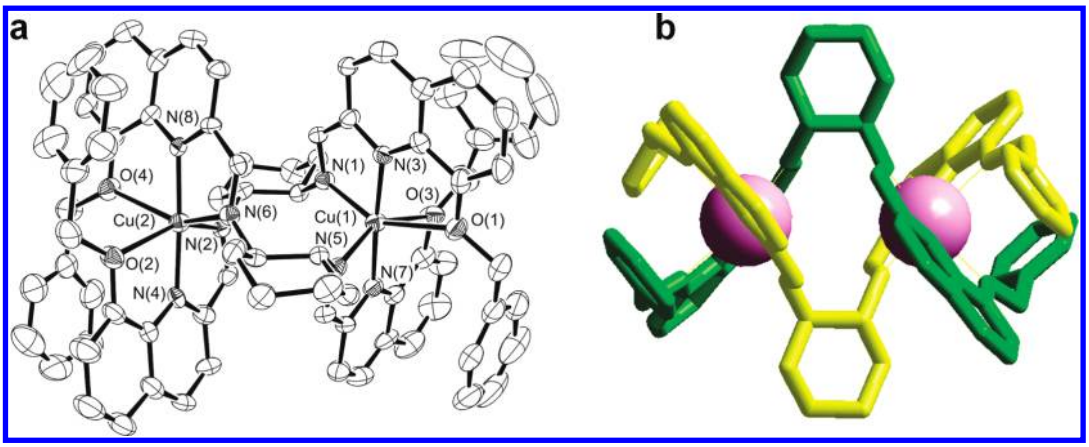

Figure 3. (a) ORTEP diagram of the *P*,*P*-$[Cu_2^{II}(^{RR}\mathbf{5})_2]^{4+}$ cationic complex (ellipsoids are drawn at the 30% probability level, names are only show for the coordinated metal centers). (b) Tube representation of the same complex, in which the two strands are presented in different colors. Cu^{II} metal centers are represented as violet spheres. The hydrogen atoms of the two strands have been omitted for clarity. The $Cu^{II}\cdots Cu^{II}$ distance is 5.05(1) Å.

Table 2. Structural Parameters Relevant to Metal−Ligand Interactions in the Double-Strand Helicate Complex *P*,*P*-$[Cu_2^{II}(^{RR}\mathbf{5})_2]^{4+}$ Obtained from $^{RR}\mathbf{5}$ and from $^{rac}\mathbf{5}$[a]

	P,*P*-$[Cu_2^{II}(^{RR}\mathbf{5})_2]^{4+}$ from $^{RR}\mathbf{5}$			*P*,*P*-$[Cu_2^{II}(^{RR}\mathbf{5})_2]^{4+}$ from $^{rac}\mathbf{5}$	
Cu(1)−N(1)	2.089(7)	Cu(2)−N(2)	2.099(7)	Cu(1)−N(1)	2.107(7)
Cu(1)−N(3)	1.934(6)	Cu(2)−N(4)	1.936(7)	Cu(1)−N(2)	1.950(7)
Cu(1)−N(5)	2.095(7)	Cu(2)−N(6)	2.105(7)	Cu(1)−N(1)′	2.107(7)
Cu(1)−N(7)	1.940(7)	Cu(2)−N(8)	1.934(6)	Cu(1)−N(2)′	1.950(7)
Cu(1)−O(1)	2.465(6)	Cu(2)−O(2)	2.480(6)	Cu(1)−O(1)	2.451(7)
Cu(1)−O(3)	2.459(6)	Cu(2)−O(4)	2.527(6)	Cu(1)−O(1)′	2.451(7)
N(1)−Cu(1)−N(3)	81.0(3)	N(2)−Cu(2)−N(4)	81.4(3)	N(1)−Cu(1)−N(2)	81.2(3)
N(1)−Cu(1)−N(5)	111.4(3)	N(2)−Cu(2)−N(6)	111.9(2)	N(1)−Cu(1)−N(1)′	110.9(3)
N(1)−Cu(1)−N(7)	100.7(3)	N(2)−Cu(2)−N(8)	99.2(3)	N(1)−Cu(1)−N(2)’	100.0(3)
N(1)−Cu(1)−O(3)	85.9(3)	N(2)−Cu(2)−O(4)	85.6(2)	N(1)−Cu(1)−O(1)′	86.1(3)
N(3)−Cu(1)−N(5)	101.2(3)	N(4)−Cu(2)−N(6)	101.0(3)	N(2)−Cu(1)−N(1)′	100.0(3)
N(3)−Cu(1)−O(1)	73.0(2)	N(4)−Cu(2)−O(2)	72.9(3)	N(2)−Cu(1)−O(1)	72.9(2)
N(3)−Cu(1)−O(3)	104.5(3)	N(4)−Cu(2)−O(4)	105.1(3)	N(2)−Cu(1)−O(1)′	105.4(2)
N(5)−Cu(1)−N(7)	80.7(3)	N(6)−Cu(2)−N(8)	81.5(3)	N(1)′−Cu(1)−N(2)′	81.2(3)
N(5)−Cu(1)−O(1)	86.3(3)	N(6)−Cu(2)−O(2)	83.1(2)	N(1)′−Cu(1)−O(1)	86.1(3)
N(7)−Cu(1)−O(1)	104.8(2)	N(8)−Cu(2)−O(2)	106.0(2)	N(2)′−Cu(1)−O(1)	105.4(2)
N(7)−Cu(1)−O(3)	73.2(3)	N(8)−Cu(2)−O(4)	72.1(3)	N(2)′−Cu(1)−O(1)′	72.9(2)
O(1)−Cu(1)−O(3)	88.5(2)	O(2)−Cu(2)−O(4)	91.7(2)	O(1)−Cu(1)−O(1)′	88.9(3)

[a] Symmetry code: (′) = $^5/_4 - x, y, {}^1/_4 - z$.

Results and Discussion

1. Structural Aspects. 1.1. Structure of the Cu^{II} Complexes. On slow diffusion of diethylether on a MeCN solution containing equimolar amounts of $Cu^{II}(CF_3SO_3)_2$ and **5** in *R* form, brown crystals of a compound of formula $[Cu_2^{II}(^{RR}\mathbf{5})_2](CF_3SO_3)_4$ were obtained. Figure 3a shows the ORTEP diagram for the cationic complex *P*,*P*-$[Cu_2^{II}(^{RR}\mathbf{5})_2]^{4+}$. Two molecules of **5** with the same configuration for the ligand stereocenters are wrapped around each other and held together by two Cu^{II} ions, to give a homochiral double helix. The double helical arrangement is put in clear evidence in Figure 3b and the *P*,*P*-$[Cu_2^{II}(^{RR}\mathbf{5})_2]^{4+}$ molecular cation exhibits D_2 molecular symmetry.

The crystal structure has the crystallographic symmetry of the $P2_12_12_1$ chiral space group, and the final Flack's parameters, −0.02(2), obtained during the structure refinement, confirms that the crystal contains only the *P*,*P*-$[Cu_2^{II}(^{RR}\mathbf{5})_2]^{4+}$ enantiomer of the molecular cation. Each Cu^{II} ion is six-coordinated through the binding of a NNO terdentate subunit (imine nitrogen atom, quinoline nitrogen atom, benzyloxy oxygen atom) from each strand. Relevant strucural parameters are reported in Table 2, together with those of the perfectly D_2 *P*,*P*-$[Cu_2^{II}(^{RR}\mathbf{5})_2]^{4+}$ enantiomer obtained from $^{rac}\mathbf{5}$ (vide infra).

The Cu^{II}−N(quinoline) distances (mean value 1.94(1) Å for both Cu centers) are notably shorter than the Cu^{II}−N(imine) ones (mean value 2.09(1) Å for Cu(1) and 2.10(1) Å for Cu(2)). On the other hand, the Cu^{II}−O distances observed here are especially large (in the range 2.46(1)−2.53(1) Å), yet lower than observed in other N_4O_2 complexes, e.g. *trans*-$[Cu^{II}(en)_2(H_2O)_2]^{2+}$ (2.60−2.62 Å)[27] and *trans*-$[Cu^{II}(cyclam)(H_2O)_2]^{2+}$ (2.55 Å),[28] which, however, exhibit a different coordination geometry (highly elongated octahedron, with oxygen atoms occupying axial positions). Moreover, each NNO set belonging to a given strand provides meridional coordination, as frequently observed in octahedral complexes in which the metal center is bound to two linear terdentate ligands. In particular, the angle between the two NNO

(27) Kuchar, J.; Cernak, J.; Massa, W. *Acta Crystallogr., Sect. C: Cryst. Struct. Commun.* **2004**, *60*, m418.
(28) Hunter, T. M.; McNae, I. W.; Liang, X.; Bella, J.; Parsons, S.; Walkinshaw, M. D.; Sadler, P. J. *Proc. Natl. Acad. Sci. U.S.A.* **2005**, *102*, 2288–2292.

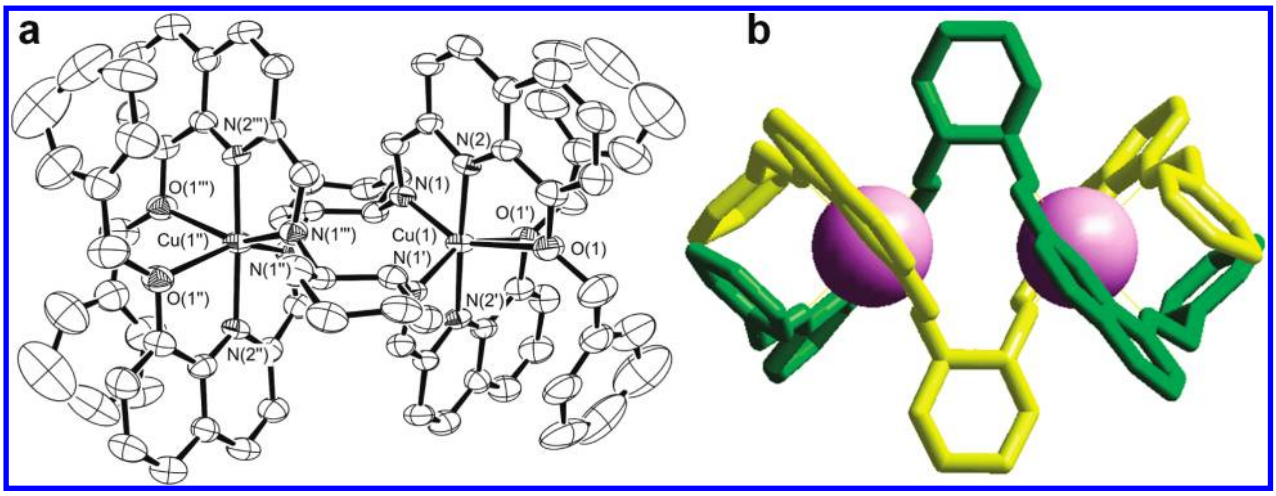

Figure 4. (a) ORTEP diagram of the *P*,*P*-$[Cu_2^{II}(^{RR}\mathbf{5})_2]^{4+}$ cationic complexes forming the $[Cu_2^{II}(^{rac}\mathbf{5})_2](CF_3SO_3)_4$ crystal obtained from $^{rac}\mathbf{5}$ (ellipsoids are drawn at the 30% probability level, atom names are shown only for atoms involved in the two metal centers, symmetry code: (′) = $^5/_4 - x, y, {}^1/_4 - z$, (″) = $^5/_4 - x, {}^1/_4 - y, z$, (‴) = $x, {}^1/_4 - y, {}^1/_4 - z$). (b) Tube representation of the same complex, in which the two strands are presented in different colors. Cu^{II} metal centers are represented as violet spheres, and the $Cu^{II}\cdots Cu^{II}$ distance is 5.04(1) Å. The crystal structure is centrosymmetric and contains both enantiomers: *P*,*P*-$[Cu_2^{II}(^{RR}\mathbf{5})_2]^{4+}$ (shown in this figure) and *M*,*M*-$[Cu_2^{II}(^{SS}\mathbf{5})_2]^{4+}$, giving rise to a racemic crystal.

planes is 86.5(1)° for the Cu(1) center and 84.6(1) for the Cu(2) center (vs a regular value of 90°).

It is worth noting the presence of well-defined face-to-face π-stacking interactions between the quinoline system of one strand and the phenyl group of the benzyloxy system of the other strand, for a total of *four*. The centroid−centroid separations between each quinoline moiety and the phenyl ring of the other strand, and the closest C···C contacts characterizing any of the four face-to-face π-stacking interactions are 3.44(1) and 3.32(1) for the first one and 3.52(1) and 3.44(1) for the second one; 3.63(1) and 3.54(1) for the third one; 3.69(1) and 3.27(1) for the fourth one. Just to make a well-known example, the separation between two planes in graphite is 3.35 Å. These $\pi-\pi$ interactions are believed to contribute substantially to the stability of the double-helical arrangement of the dicopper(II) complex. It appears also that it is the folding of the phenyl ring of each benzyloxy system, needed for establishing $\pi-\pi$ interactions, that brings the oxygen atoms to an interaction distance with the Cu^{II} centers. Such interactions are in any case well-accepted by each Cu^{II} ion, which arranges nitrogen donor atoms around in a way that leaves room for the coordination of the two oxygen atoms. The rather large $Cu^{II}\cdots Cu^{II}$ distance (5.05 Å), as well as coordinative saturation, rule out the establishing of any metal−metal interaction.

Very interestingly, on slow diffusion of diethylether on a solution containing equimolar amounts of $Cu^{II}(CF_3SO_3)_2$ and $^{rac}\mathbf{5}$, racemic red crystals of a compound of formula $[Cu_2^{II}(^{rac}\mathbf{5})_2]$ $(CF_3SO_3)_4$ were obtained. The crystal structure is rather complicated, being constituted by two similar but nonsymmetrically equivalent dinuclear homochiral double-helicate species. One of the two independent molecular cations shows some unexpected geometrical features (as a pronounced nonplanarity for the aromatic rings) that have been ascribed to the poor X-ray diffraction quality of the available crystals and we will consider in the following discussion only the features of the molecule better characterized with the diffraction data.

Figure 4a shows the ORTEP diagram for the dinuclear homochiral *P*,*P*-$[Cu_2^{II}(^{RR}\mathbf{5})_2]^{4+}$ double-strand cationic complex that occurs in the $[Cu_2^{II}(^{rac}\mathbf{5})_2]$ $(CF_3SO_3)_4$ crystal obtained from $^{rac}\mathbf{5}$, while Figure 4b illustrates that the double-helix arrangement of the two strands around the two Cu^{II} is the same as observed in the Cu^{II} crystal described above (obtained from $^{RR}\mathbf{5}$, see Figure 3).

The *P*,*P*-$[Cu_2^{II}(^{RR}\mathbf{5})_2]^{4+}$ molecular cation exhibits a perfect D_2 molecular symmetry because the centroid of the molecule coincides with the crystallographic position in which three perpendicular 2-fold axes cross.

The coordination around the two symmetrically equivalent Cu^{II} ions is the same as observed in the crystal obtained from $^{RR}\mathbf{5}$ (Table 2), and each NNO set belonging to a given strand is still placed accordingly to a meridional coordination: the angle between the two NNO planes is 86.7(1)° (vs a regular value of 90°). To the best of our knowledge, the complexes discussed above represent the first examples of dicopper(II) double-strand helicate complexes exhibiting local octahedral geometry.

Also in the crystal obtained from $^{rac}\mathbf{5}$, there are well-defined face-to-face π-stacking interactions between the quinoline system of one strand and the phenyl group of the benzyloxy system of the other strand, for a total of four. Due to the crystallographic symmetry of the molecule, all these interactions are symmetrically equivalent: all the four centroid−centroid separations between quinoline and phenyl are 3.47(1) Å; all the four closest C···C contacts are 3.32(1) Å. Thus, these structural parameters define intramolecular interactions completely similar to those observed in the crystal from $^{RR}\mathbf{5}$.

Quite interestingly, the $[Cu_2^{II}(^{rac}\mathbf{5})_2](CF_3SO_3)_4$ crystal (centrosymmetric crystal structure, *Fddd* space group) is a racemic mixture of the two enantiomeric homochiral isomers. Therefore, for any binuclear double-strand molecule formed by two ligands **5** having the *trans*-1,2-cyclohexanediamine subunits in the *R* form there exists the corresponding double-strand isomer with ligands **5** having the *trans*-1,2-cyclohexanediamine subunits in the *S* form. Then, the crystal contains both the *P*,*P*-$[Cu_2^{II}(^{RR}\mathbf{5})_2]^{4+}$

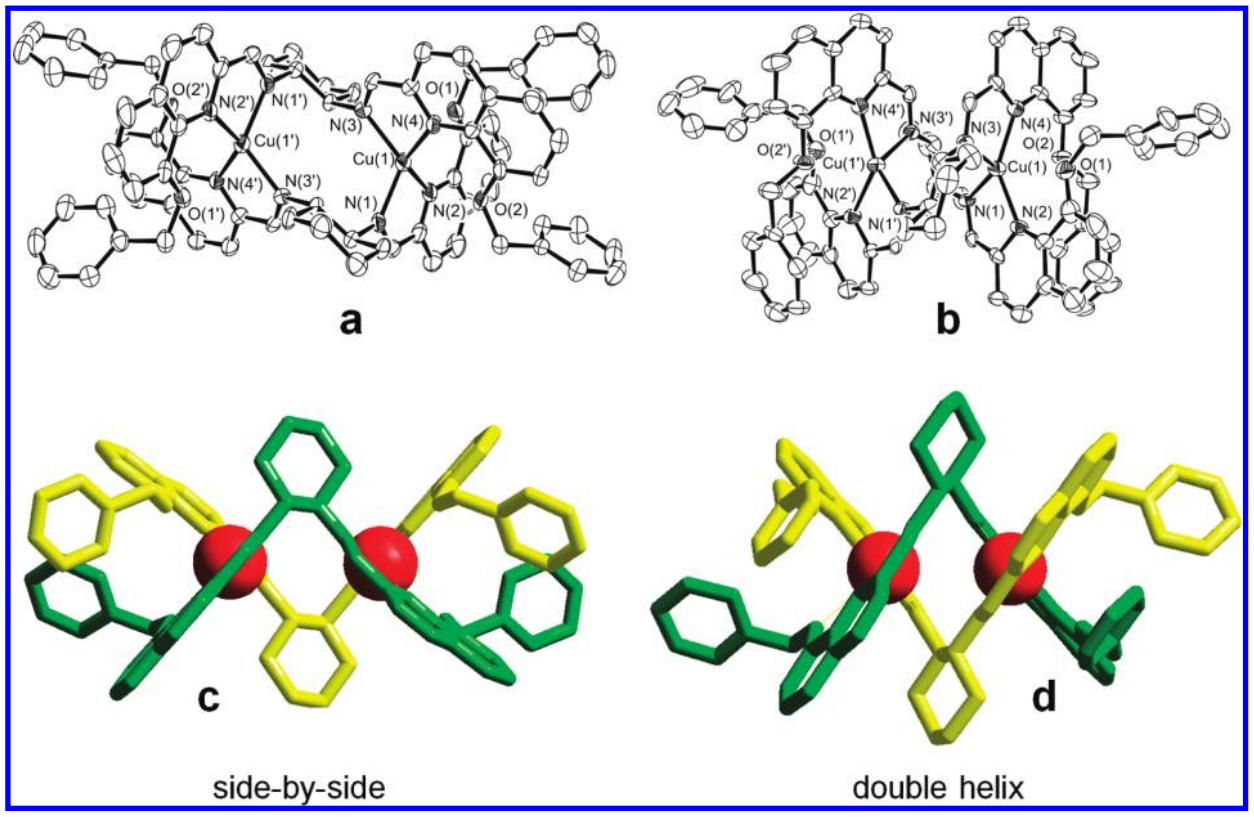

Figure 5. (a) ORTEP diagrams for $[Cu_2^I(^{RR}\mathbf{5})(^{SS}\mathbf{5})]^{2+}$ (symmetry code: (′) = $2-x, 1-y, 2-z$). (b) ORTEP diagrams and M,M-$[Cu^I(^{RR}\mathbf{5})_2]^{2+}$ (symmetry code: (′) = $^3/_2 - x, y, ^3/_2 - z$). Both ORTEP diagrams are drawn at the 30% probability level with atom names reported only for the metal centers and hydrogen atoms omitted for clarity. (c and d) Tube representations of the same complexes that emphasize the different structural architectures (side-by-side vs double helix). The two Cu^I centers (red spheres) are 4.99(1) Å far away in the side-by-side complex, whereas they are separated by only 3.89(1) Å in the helicate complex.

and the M,M-$[Cu_2^{II}(^{SS}\mathbf{5})_2]^{4+}$ enantiomers of the molecular complex in a 1:1 ratio.

"Chiral-directed self-assembling" of chiral ligands around metal centers is a well-known process that leads to the formation of homochiral double-strand helicate complexes also in the presence of a racemic mixture of ligands.[16] This process has been identified for binuclear double-strand molecular complexes having tetrahedral metal centers.[16] This study has demonstrated that the principle of homochiral recognition in helicate self-assembling can be extended to octahedral metal centers.

1.2. Structure of the Cu^I Complexes Obtained from the Racemic Form of 5. The coordinating behavior of ligand **5** with the Cu^I cation is peculiar. On slow diffusion of diethylether on a solution containing equimolar amounts of $Cu^I(MeCN)_4ClO_4$ and $^{rac}\mathbf{5}$, two different molecular and crystal structures were obtained, depending upon the used solvent (whether THF or MeCN).

Both crystals contain dinuclear molecular cations consisting of two molecules of the ligand **5** chelated to two Cu^I centers. However, striking chiral and topological differences were observed: (i) the blue $[Cu_2^I(^{rac}\mathbf{5})_2](ClO_4)_2 \cdot 2(Et_2O)$ crystal obtained from MeCN contained isolated diethylether molecules, perchlorate counterions, and the heterochiral dimeric molecular cations of formula $[Cu_2^I(^{RR}\mathbf{5})(^{SS}\mathbf{5})]^{2+}$, in which the two enantiomeric forms of the ligand **5** are present in the same dinuclear Cu^I complex and are disposed according to a side-by-side arrangement; (ii) the brown $[Cu_2^I(^{rac}\mathbf{5})_2](ClO_4)_2 \cdot H_2O$ crystal obtained from THF contained isolated water molecules, perchlorate counterions and a racemic mixture of the homochiral dimeric compounds M,M-$[Cu^I(^{RR}\mathbf{5})_2]^{2+}$ and P,P-$[Cu_2^I(^{SS}\mathbf{5})_2]^{2+}$, in which the two strands are arranged as a double helix. Figure 5 shows the ORTEP diagram for the two different dimeric cationic complexes with a tube rendering further used to emphasize the two different structural arrangements.

Table 3. Selected Bond Length (Å) and Bond Angles (deg) around the Cu^I Center in $[Cu_2^I(^{RR}\mathbf{5})(^{SS}\mathbf{5})]^{2+}$ and M,M-$[Cu_2^I(^{RR}\mathbf{5})_2]^{2+}$ Molecular Cations

	$[Cu_2^I(^{RR}\mathbf{5})(^{SS}\mathbf{5})]^{2+}$	M,M-$[Cu_2^I(^{RR}\mathbf{5})_2]^{2+}$
Cu(1)−N(1)	2.016(7)	2.024(11)
Cu(1)−N(2)	2.112(7)	2.082(12)
Cu(1)−N(3)	2.026(7)	2.077(11)
Cu(1)−N(4)	2.109(8)	2.049(12)
N(1)−Cu(1)−N(2)	81.0(3)	82.1(5)
N(1)−Cu(1)−N(3)	120.2(3)	121.2(4)
N(1)−Cu(1)−N(4)	123.7(3)	123.0(4)
N(2)−Cu(1)−N(3)	125.4(4)	109.2(5)
N(2)−Cu(1)−N(4)	130.5(3)	142.3(5)
N(3)−Cu(1)−N(4)	81.7(3)	83.0(5)

In both molecular structures, the two Cu^I centers are symmetrically equivalent and are coordinated by four nitrogen atoms, two from one strand and two from the other, according to a rather distorted tetrahedral geometry. Features for the coordination of the metal centers are reported in Table 3.

The shorter distances of the Cu−N(imine) bonds with respect to the Cu−N(quinoline) bonds, observed for Cu^{II} complexes (vide supra), remain evident only for the side-by-side heterochiral $[Cu_2^I(^{RR}\mathbf{5})(^{SS}\mathbf{5})]^{2+}$ molecular

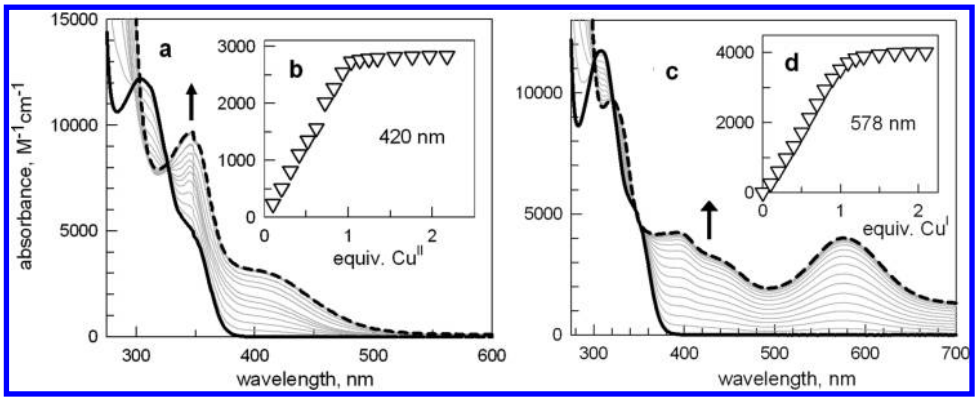

Figure 6. (a) Family of spectra recorded over the course of the titration of a 1.00×10^{-4} solution of ^{rac}**5**: with a 1.0×10^{-2} MeCN solution of $Cu^{II}(CF_3SO_3)_2$: (thick solid line) spectrum of ^{rac}**5** prior to the titration; (thick dashed line) spectrum after the addition of 2.5 equiv of Cu^{II}, to which a bright yellow color corresponds; (c) with a 1.0×10^{-2} MeCN solution of $[Cu^{I}(MeCN)_4]ClO_4$; (thick solid line) spectrum of ^{rac}**5** prior to the titration; (thick dashed line) spectrum after the addition of 2.5 equiv of Cu^{I}. (b and d) Insets titration profiles at selected wavelengths.

complex, even if to a lesser extent. On the contrary, the homochiral *M*,*M*-$[Cu^{I}(^{RR}\mathbf{5})_2]^{2+}$ molecular complex (and the corresponding *P*,*P*-$[Cu^{I}(^{SS}\mathbf{5})_2]^{2+}$ enantiomer) shows close $Cu^{I}-N$ bond distances, with the $Cu^{I}-N$(quinoline) distances ranging over an interval (2.05−2.08 Å) typically observed in copper(I) complexes with pyridines under unconstrained conditions (es. $[Cu^{I}(py)_4]^{+}$, $Cu^{I}-N$: 2.06 Å).[29]

For both complexes, a nearly regular tetrahedral geometry is observed: for instance, the value for the Φ angle, described as the dihedral angle between the two chelate ligand planes, is 87.6(1) for both Cu^{I} centers in the side-by-side $[Cu_2^{I}(^{RR}\mathbf{5})(^{SS}\mathbf{5})]^{2+}$ molecular cation and 79.6(1)° for both Cu^{I} centers in the double helix *M*,*M*-$[Cu_2^{I}(^{RR}\mathbf{5})_2]^{2+}$ complex (Φ is 0° or 180° for a square planar coordination geometry; 90° for tetrahedral coordination geometry). The oxygen atoms of the benzyloxy substituents are located at 2.89(1) and 2.83(1) Å from the Cu^{I} ion in $[Cu_2^{I}(^{RR}\mathbf{5})(^{SS}\mathbf{5})]^{2+}$ and 2.79(1) and 2.87(1) Å from the Cu^{I} ion in *M*,*M*-$[Cu_2^{I}(^{RR}\mathbf{5})_2]^{2+}$ molecular cation, a circumstance which excludes any coordinative interaction. The two metal centers are 4.99 Å far away in the side-by-side complex $[Cu_2^{I}(^{RR}\mathbf{5})(^{SS}\mathbf{5})]^{2+}$, whereas they are much closer (3.89 Å) in the helicate complex *M*,*M*-$[Cu_2^{I}(^{RR}\mathbf{5})_2]^{2+}$.

It is worth noting that, as the heterochiral $[Cu_2^{I}(^{RR}\mathbf{5})(^{SS}\mathbf{5})]^{2+}$ molecular complex exhibits *Ci* molecular symmetry, the two ligands **5** are two enantiomers bound to the same couple of Cu^{I} centers without forming a double-helix. On the contrary, as the homochiral *M*,*M*-$[Cu_2^{I}(^{RR}\mathbf{5})_2]^{2+}$ molecular complex (and the corresponding *P*,*P*-$[Cu_2^{I}(^{SS}\mathbf{5})_2]^{2+}$ enantiomer) exhibits C_2 molecular symmetry, the two strands connected to the same Cu^{I} couple have the same configuration and this addresses to a homochiral double helix molecular architecture.

Interestingly, no intramolecular face-to-face π-stacking interactions are observed in the heterochiral $[Cu_2^{I}(^{RR}\mathbf{5})(^{SS}\mathbf{5})]^{2+}$ dinuclear complex, where the two strands are arranged side-by-side. On the other hand, only two of the four possible face-to-face π-stacking interactions between quinoline and phenyl rings are established in the homochiral *M*,*M*-$[Cu_2^{I}(^{RR}\mathbf{5})_2]^{2+}$ dinuclear complex that forms a double helix arrangement. However, these two symmetrically related interactions are less intense than in the dicopper(II) helicates of **5**, as evidenced by the larger value for the centroid−centroid separation: 4.06(1) Å. In the same way, the closest C···C contacts (3.43(1) Å) are appreciably longer.

The possibility to obtain a dicopper(I) molecular complex both as a dimeric helical species and a nonhelical side-by-side dimeric species was previously observed for the $[Cu_2^{I}(\mathbf{3})_2]^{2+}$, where the two forms coexisted in the same cell.[13] Both side-by-side and double-helix arrangements allow a very similar tetrahedral coordination for Cu^{I} centers in the molecular cation obtained from ligand **5** and the energies involved in the formation of the two structurally different dimers should be rather close. In fact, if the double helicate complex profits from two π−π stacking interactions between aromatic subunits, but it should experience more intense electrostatic repulsions between the closer metal centers.

The behavior of Cu^{I} as well as of Cu^{II} complexes emphasizes that homochirality is a stringent prerequisite to form double-strand helicate complexes. Actually, only homochiral dimeric complexes of tetrahedrally coordinated Cu^{I} form double helix molecules: the double helix displays *M* handedness when the homochiral ligand strands are in the *R* forms, whereas it exhibits *P* handedness when the homochiral ligand strands are in the *S* forms. Such a relationship between the ligand configurations and the shape of the double helix has been clearly established,[16] and it has been later documented for other complexes of bis-bidentate ligands based on the *trans*-1,2-cyclohexanediamine subunit.[13−15] This work has shown that an opposite relation holds for homochiral dimeric double helicate complexes with octahedrally coordinated Cu^{II} centers, for which the two homochiral double helicate species *P*,*P*-$[Cu_2^{II}(^{RR}\mathbf{5})_2]^{4+}$ and *M*,*M*-$[Cu_2^{II}(^{SS}\mathbf{5})_2]^{4+}$ are formed.

2. Redox Behavior of Cu^{II} and Cu^{I} Complexes. 2.1. Nature and Stability of the Complexes in MeCN Solution: Cu^{II} Complex. In order to get information on the stoichiometry and stability of the Cu^{II} complex in MeCN, a solution 10^{-4} M in ^{rac}**5** was titrated with a standard solution of $Cu^{II}(CF_3SO_3)_2$. Figure 6a shows the family of spectra obtained over the course of the titration.

(29) Horvat, G.; Portada, T.; Stilinovic, V.; Tomisic, V. *Acta Crystallogr., Sect. E: Struct. Rep. Online* **2007**, *63*, m1734.

The uncomplexed ligand ^{rac}**5** shows an intense absorption band at 310 nm, with a shoulder at 350 nm, assigned to transitions within the imine−pyridine system (thick solid line). On Cu^{II} addition, the two bands are substantially red-shifted, as a consequence of the interaction of the metal ion with imine and pyridine nitrogen atoms, while the solution takes a bright yellow color. The titration profile based on the absorbance at 420 nm, displayed in Figure 6b, clearly indicates the formation of a complex species with 1:1 metal/ligand ratio. Such a value is consistent with the formation of both the mononuclear $[Cu^{II}(\mathbf{5})]^{2+}$ and the dinuclear $[Cu_2^{II}(\mathbf{5})_2]^{4+}$ complex. The absence of curvature in the profile indicates the formation of an especially stable complex ($K \geq 10^6$ for the mononuclear species), and in any case ensures that, in a solution containing equimolar amounts of metal and ligand, in the envisaged range of concentration, the complex is present at 100%.

More direct information on the nature of the Cu^{II} complex in MeCN was obtained from ESI mass experiments (see Figure S8 in the Supporting Information). In particular, the mass spectrum of a solution containing equimolar amounts of ^{rac}**5** and of $Cu^{II}(CF_3SO_3)_2$ showed a peak at 333.8 m/z, which corresponds to the monomeric complex $[Cu^{II}(\mathbf{5})]^{2+}$. In particular, the isotope pattern showed a peak-to-peak separation of 0.5 m/z, as expected for a monomeric species. This indicates that the dimeric double helicate complex, observed in the solid state, is not very stable in MeCN, and the Cu^{II} ion prefers to form with **5** a monomeric species, which may be stabilized through the coordination of one or two solvent molecules, according to a square pyramidal or an octahedrally elongated geometry. However, the presence at the equilibrium of a small portion of the dinuclear complex cannot be ruled out, because it would show, too, a peak at 333.8 m/z (= 1335.2/4), while the peaks of the isotopic pattern, with a peak-to-peak separation of 0.25 m/z, could be hidden by those of the monomeric complex. Further convincing pieces of information on the predominance of the mononuclear complex in MeCN solution will be provided by electrochemical investigations (vide infra).

2.2. Nature and Stability of the Complexes in MeCN Solution: Cu^{I} Complex. An MeCN solution of ^{rac}**5** was also titrated with a standard solution of $[Cu^{I}(MeCN)_4]ClO_4$. Figure 6c shows the family of spectra obtained over the course of the titration. On metal addition, a red-shift of the bands at 300−330 nm is observed, more pronounced than for Cu^{II}, and, more significantly, a new band develops at 580 nm, while the solution takes an intense blue color. The new band is related to the formation of a four-coordinated Cu^{I} complex, of tetrahedral geometry, and has metal-to-ligand charge transfer (MLCT) nature. Looking at the titration profile in Figure 6b, it is observed that (i) saturation is achieved on addition of 1 equiv of Cu^{I} and (ii) a slight, still discernible, slope change occurs at 0.5 equiv. This state of affairs can be accounted for on assuming the occurrence of the following stepwise equilibria:

$$Cu^{+} + 2\mathbf{L} \leftrightarrows [Cu^{I}(\mathbf{L})_2]^{+} \qquad K_{12} \qquad (1)$$

$$2Cu^{+} + 2\mathbf{L} \leftrightarrows [Cu^{I}(\mathbf{L})_2]^{2+} \qquad K_{22} \qquad (2)$$

Indeed, the best fitting of titration data over the 275−700 nm interval, using a nonlinear least-squares procedure,[30] was obtained on the basis of equilibria 1 and 2, for which the following constants were calculated: $\log K_{12} = 10.05 \pm 0.03$ and $\log K_{22} = 15.89 \pm 0.03$. From $\log K$ values, it can be calculated that in a MeCN solution 10^{-4} M both in Cu^{I} and in ^{rac}**5** the dinuclear complex $[Cu^{I}(\mathbf{L})_2]^{2+}$ is formed at 85%.

The formation of the dinuclear complex was confirmed by ESI mass experiments. In fact, the mass spectrum of a MeCN solution containing equimolar amounts of ^{rac}**5** and of $[Cu^{I}(MeCN)_4]ClO_4$ showed (i) a peak at 1434.6 m/z, with an isotope pattern with a peak-to-peak separation of 1.0 m/z, corresponding to $[Cu_2^{I}(\mathbf{L})_2(ClO_4)]^{+}$ and (ii) a peak 667.4 m/z, with a well-defined peak-to-peak separation of 0.5 m/z in the isotope pattern, which corresponds to $[Cu_2^{I}(\mathbf{L})_2]^{2+}$ (see Figures S6 and S7 of the Supporting Information).

Similar experiments were carried out on a MeCN solution containing equimolar amounts of $[Cu^{I}(MeCN)_4]ClO_4$ and the *R* form of **5**. The formation of the two species $[Cu^{I}(\mathbf{L})_2]^{+}$ and $[Cu_2^{I}(\mathbf{L})_2]^{2+}$ was ascertained with values of equilibrium constants ($\log K_{12} = 10.11 \pm 0.05$, $\log K_{22} = 16.00 \pm 0.03$) almost coincident with those determined for ^{rac}**5**. In this case, due to the presence in solution of the *R* form of the ligand, only the helicate complex M,M-$[Cu_2^{I}(^{RR}\mathbf{5})_2]^{2+}$ should form. However, convincing information about the nature of the species present in solution has been provided by ^{1}H and ^{13}C NMR spectra on CD_3CN solutions obtained by dissolving crystalline salts of $[Cu_2^{I}(^{rac}\mathbf{5})_2]^{2+}$ and M,M-$[Cu_2^{I}(^{RR}\mathbf{5})_2]^{2+}$. In particular, the spectra of both solutions showed identical patterns, with the same chemical shifts for ^{1}H and ^{13}C spectra. This points toward the existence of only one main species in acetonitrile solution, common to both systems, and, considering that in the solution of Cu^{I} and ^{RR}**5** only the helicate species M,M-$[Cu_2^{I}(^{RR}\mathbf{5})_2]^{2+}$ is present, one should conclude that also the solution of the $[Cu^{I}(^{rac}\mathbf{5})_2]^{2+}$ complex (racemic) contains as a main component the helicate species M,M-$[Cu_2^{I}(^{RR}\mathbf{5})_2]^{2+}$ and P,P-$[Cu_2^{I}(^{SS}\mathbf{5})_2]^{2+}$. NMR spectral differences between helical and side-by-side dicopper(I) complexes have been discussed in detail for system **3**.[14]

2.3. Electrochemical Behavior of the Cu^{II} Complex. Figure 7a displays the CV profile obtained at a working platinum electrode for a MeCN solution containing equimolar amounts of ^{rac}**5** and $Cu^{II}(CF_3SO_3)_2$, at the potential scan rate of 50 mV s^{-1}.

On the first reduction scan (solid line), a single peak is observed at −5 mV; then, in the reverse oxidation scan, two peaks of lower intensity develop, at 190 and 450 mV (thus separated by 260 mV). This behavior can be accounted for on the basis of the square scheme featured in Figure 8.

The solution contains the Cu^{II} complex as a monomer, $[Cu^{II}(\mathbf{L})]^{2+}$, at least as a predominant species, as indicated by ESI mass studies. After the reduction at the electrode (upper solid arrow in the square diagram), two mononuclear complexes $[Cu^{I}(\mathbf{L})]^{+}$ assemble to give the dinuclear species $[Cu_2^{I}(\mathbf{L})_2]^{2+}$, according to step a, dashed

(30) (a) Gans, P.; Sabatini, A.; Vacca, A. *Talanta* **1996**, *43*, 1739–1753. (b) http://www.hyperquad.co.uk/index.htm (accessed October **2009**).

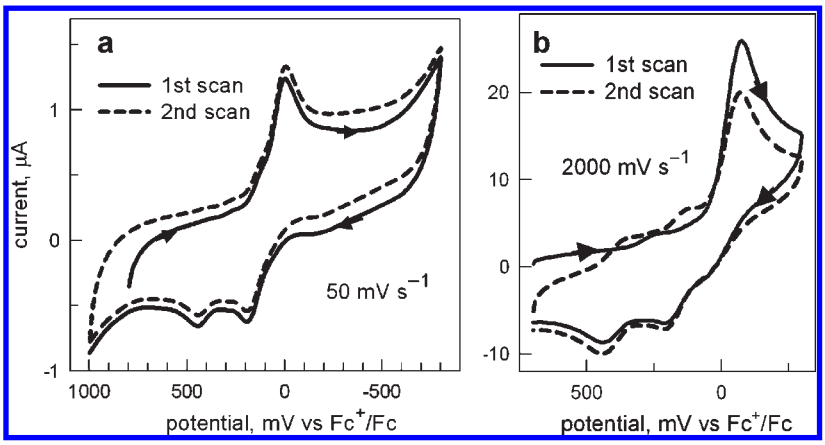

Figure 7. CV profiles for an MeCN solution 1×10^{-3} M both in ^{rac}**5** and in $Cu^{II}(CF_3SO_3)_2$. Platinum working electrode: (a) potential scan rate 50 mV s^{-1} (second scan profile (dashed line) has been shifted up of 0.05 μA for clarity); (b) potential scan rate 2000 mV s^{-1}.

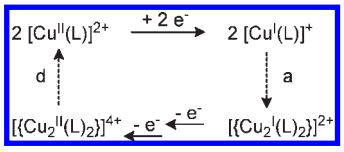

Figure 8. Square scheme for interpreting the CV profiles illustrated in Figure 7. Solid arrows indicate electrode processes, and dashed arrows show the assembling (a) and disassembling (d) processes, which follow the redox changes.

arrow down. Then, in the reverse scan, each Cu^I center undergoes independent one-electron oxidation to Cu^{II}, while the dinuclear complex maintains its integrity. It has to be noted that the oxidation of the first Cu^I center takes place within the repulsive electrical field exerted by the proximate Cu^I ion, while the oxidation of the second Cu^I center feels the repulsion of the doubly positively charged cation Cu^{II}, which reflects the potential increase of 260 mV (an advantage of 36 mV for the first oxidation step is in any case expected due to a statistical effect).[31] In any case, the electrostatic repulsion between metal centers is masked to some extent by solvation.[32] The profile of the second scan (dashed line in Figure 7) superimposes on the profile of the first scan: this indicates that the fully oxidized dinuclear complex, $[Cu_2^{II}(\mathbf{L})_2]^{4+}$, disassembles in the time scale of the CV experiment. Considering that about 1000 mV separates the potential of the second oxidation peak from the potential guessed for the development of the first reduction peak, it derives that, at the employed scan rate of 50 mV s^{-1}, the disassembling process takes place in less than 20 s.

Figure 7b shows the CV profiles taken at the highest potential scan rate available to our apparatus: 2000 mV s^{-1}. The first scan (solid line) is quite similar to that taken at 50 mV s^{-1}. However, in the second scan (dashed line), two peaks of moderate intensity develop at 420 and 170 mV, which are ascribed to the two-step one-electron reduction of the dinuclear complex, $[Cu_2^{II}(\mathbf{L})_2]^{4+}$, not yet disassembled. The more cathodic peak corresponds to the two-electron reduction of the mononuclear complex still present in overwhelming concentration: it originates from (i) the disassembling of the $[Cu_2^{II}(\mathbf{L})_2]^{4+}$ species in the Nernst layer and (ii) from the diffusion from the solution. In any case, the time necessary for moving from the second oxidation peak to the first reduction peak is ca. 0.4 s, a quantity which can provide a rough estimate of the time scale of $[Cu_2^{II}(\mathbf{L})_2]^{4+}$ disassembling.

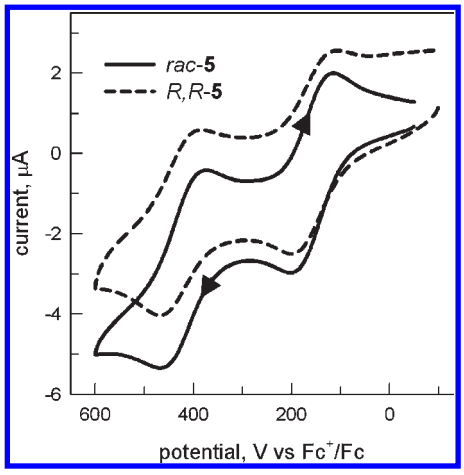

Figure 9. Cyclic voltammetry profiles for an MeCN solution 1×10^{-3} M in $[Cu^I(MeCN)_4]ClO_4$ and in ^{rac}**5** (solid line) and 1×10^{-3} M in $[Cu^I(MeCN)_4]ClO_4$ and in ^{RR}**5** (dashed line): platinum working electrode, potential scan rate 100 mV s^{-1}.

2.4. Electrochemical Behavior of Cu^I Complexes. Figure 9 shows the CV profile, taken at 100 mV s^{-1}, for a solution 10^{-3} M in both ^{rac}**5** and $[Cu^I(MeCN)_4]ClO_4$ (solid line). It is calculated from pertinent log K values that the $[Cu_2^I(\mathbf{L})_2]^{2+}$ complex is present at 92%. The oxidation profile displays two peaks separated by 260 mV, while the reduction profile shows a fully reversible pattern, with the same peak separation. This behavior indicates that the $[Cu_2^I(\mathbf{L})_2]^{2+}$ complex first undergoes two consecutive one-electron oxidation processes, to give the $[Cu_2^{II}(\mathbf{L})_2]^{4+}$ species. This species is able to maintain its full integrity over the time scale of the CV experiment (down to the slowest explored scan rate 20 mV s^{-1}). This would suggest that this species possesses a kinetic stability distinctly higher than that obtained from $[Cu^{II}(\mathbf{L})]^{2+}$, following reduction and oxidation processes, as illustrated in the square scheme in Figure 8.

Figure 9 reports also, as a dashed line, the CV profile obtained, under the same conditions, with the Cu^I complex of the *R* form of **5**, which is known to exist as a

(31) Richardson, D. E.; Taube, H. *Inorg. Chem.* **1981**, *20*, 1278–1285.
(32) Canard, G.; Piguet, C. *Inorg. Chem.* **2007**, *46*, 3511–3522.

double-strand helicate. It is observed that this profile is superimposable with that obtained with the racemic form. This confirms the hypothesis that also the racemic $[Cu_2^I(^{rac}\mathbf{5})_2]^{2+}$ complex exists in MeCN solution as *M*, *M*-$[Cu_2^I(^{RR}\mathbf{5})_2]^{2+}$ and *P*,*P*-$[Cu_2^I(^{SS}\mathbf{5})_2]^{2+}$ double helicate species. On the other hand, if the racemic $[Cu_2^I(^{rac}\mathbf{5})_2]^{2+}$ species were present in the $[Cu_2^I(^{RR}\mathbf{5})(^{SS}\mathbf{5})]^{2+}$ side-by-side arrangement, in which the Cu···Cu distance is more than 1 Å larger than in the helicate, a distinctly smaller separation of the oxidation and reduction peaks would be expected, due to the reduced intensity of electrostatic repulsions.

Conclusion

We have reported the new helicand **5**, which contains two sets of NNO donor atoms and is capable of forming double-strand homodimetallic helicates with both Cu^I and Cu^{II}. In particular, **5** acts as a bis-bidentate ligand when reacting with Cu^I, which adopts a distorted tetrahedral geometry through the coordination by four sp^2 hybridized nitrogen atoms, while it behaves as a bis-terdentate ligand, when it reacts with Cu^{II}, which profits also from the binding of two benzyloxy oxygen atoms to reach a very distorted octahedral coordination. In particular, the $[Cu_2^{II}(\mathbf{5})_2]^{4+}$ complex is the first double-strand helicate containing two Cu^{II} octahedral centers. It should be noted that the dicopper(II) helicate complex in the solid state is stabilized also by an intricate system of $\pi-\pi$ interactions between aromatic subunits. However, this species is not stable enough to resist the competition for the metal by MeCN, the solvent used for electrochemical studies, and the monomeric complex is present in solution. This leads to the classical assembling−disassembling process switched through the Cu^{II}/Cu^I couple, as observed in CV experiments on a solution of the Cu^{II} complex. On the other hand, the dinuclear Cu^{II} complex obtained through a CV experiment on a solution of the dinuclear Cu^I species shows a relatively high stability and lasts in solution in the time scale of the CV experiment performed at a potential scan rate of 20 mV s^{-1}, to which a lifetime ≥20 s corresponds. Such stability is kinetic in nature and probably reflects the slow unpacking of the two strands held together not only by the metal−ligand bonds, but also by interligand intracomplex $\pi-\pi$ interactions.

Moreover, this work has thrown further light on the factors governing the formation of chiral double-strand helicates. While it is well-known that in a double helix the two strands must have the same handedness, it has been shown here that, for ligand **5**, which presents two chiral centers, two strands of the same chirality, either *R* or *S*, self-recognize each other, to wrap around two metal ions, in order to give a double helix. However, the double helix may not be the most stable arrangement, a side-by-side ligand architecture being thermodynamically favored, under given conditions,. Noticeably, the side-by-side architecture requires the coupling of a *R* with a *S* strand. Thus, in order to address the formation of a double helicate, a pure enantiomeric form of the ligand, either *R* or *S*, should be used.

Acknowledgment. The financial support of the Italian Ministry of University and Research and of the University of Pavia is gratefully acknowledged.

Supporting Information Available: X-ray crystallographic files in CIF format for the complex salts: $Cu_2^{II}(^{RR}\mathbf{5})_2](CF_3SO_3)_4$, $Cu_2^{II}(^{rac}\mathbf{5})_2](CF_3SO_3)_4$, $[Cu_2^I(^{rac}\mathbf{5})_2](ClO_4)_2\cdot 2Et_2O$, $[Cu_2^I(^{rac}\mathbf{5})_2](ClO_4)_2\cdot H_2O$. Details on synthesis of **5**; ESI-MS spectra of $[Cu_2^I(^{RR}\mathbf{5})_2]^{2+}$ and of $[Cu^{II}(^{RR}\mathbf{5})]^{2+}$ in $CHCl_3$. CV profile for a solution of the Cu^{II} complex of $^{rac}\mathbf{5}$ in CH_2Cl_2. This material is available free of charge via the Internet at http://pubs.acs.org.